Geophysical Research Letters

RESEARCH LETTER
10.1029/2025GL118812

Special Collection:
Modeling of Geological Hazards in Complex Environments

New Analytical Model for Forecasting Turbidity Current Run-Up Heights: Implications for Risk Assessment of Seafloor Infrastructure on Submarine Slopes

Ru Wang[1], Mia Hughes[1], Jeff Peakall[1], David M. Hodgson[1], Ed Keavney[1], Helena C. Brown[1], and Gareth M. Keevil[1]

[1]School of Earth & Environment, University of Leeds, Leeds, UK

Abstract Turbidity currents are destructive flows that are hazardous to critical seafloor infrastructure on submarine slopes because run-up heights can be 10–100s of meters, as their relative density is 2–3 orders of magnitude lower than terrestrial flows. Currently, risk analysis is hindered by poor prediction of run-up heights that are mainly derived from confined 2D experiments, and/or numerical models, and are restricted to a specific configuration whereby the flow strikes topographic barriers orthogonally. Here, a new analytical model is presented, informed by and validated against physical experiments, which predicts run-up heights for flows encountering three-dimensional slopes as a function of any slope angle, and incidence angle, of the impinging turbidity current. This has important implications for reducing geohazards by informing routing and positioning of seafloor infrastructure, and for more accurately interpreting submarine landscapes and their deposits.

Plain Language Summary The planet's seafloor, including submarine slopes, is increasingly instrumented with critical infrastructure. These regions are at risk from destructive underwater "avalanches" that have the potential to run-up topography for long distances. Currently, our estimates of run-up height are restricted to a specific scenario: flows orthogonal to slopes. Here, we present a new analytical model validated by a suite of physical experiments that accounts for a wide range of flow-slope interactions to improve predictions of run-up height. The model can be applied during planning for future seafloor developments, informing revised risk assessments of existing infrastructure.

Key Points:

- Existing 2D predictive models based on frontal topographic configurations markedly underestimate turbidity current run-up heights
- A critical slope gradient exists whereby the maximum run-up height reaches its highest value, when the flow incidence angle is kept uniform
- A new analytical model validated to experimental data can help to inform risk assessment and planning of critical seafloor infrastructure

Supporting Information:

Supporting Information may be found in the online version of this article.

Correspondence to:

R. Wang,
earrwa@leeds.ac.uk

Citation:

Wang, R., Hughes, M., Peakall, J., Hodgson, D. M., Keavney, E., Brown, H. C., & Keevil, G. M. (2026). New analytical model for forecasting turbidity current run-up heights: Implications for risk assessment of seafloor infrastructure on submarine slopes. *Geophysical Research Letters*, *53*, e2025GL118812. https://doi.org/10.1029/2025GL118812

Received 15 AUG 2025
Accepted 12 JAN 2026

Author Contributions:

Conceptualization: Ru Wang, Mia Hughes
Data curation: Ru Wang
Formal analysis: Ru Wang
Funding acquisition: David M. Hodgson
Investigation: Ru Wang
Methodology: Ru Wang, Mia Hughes, Ed Keavney, Helena C. Brown, Gareth M. Keevil

1. Introduction

Critical seafloor infrastructure installations are rapidly increasing across the planet, including on submarine slopes. This infrastructure, such as hydrocarbon pipelines and telecommunication cables (e.g., Bricheno et al., 2024), is at risk from damage by destructive turbidity currents, which are gravity-driven, sediment-laden flows (e.g., B. Kneller & Buckee, 2000). Turbidity current dynamics are strongly influenced by seafloor topography (e.g., B. Kneller et al., 1991; B. C. Kneller et al., 1997), which alters flow velocity, sediment concentration profiles, and therefore sediment transport capacity (e.g., Edwards et al., 1994). Due to their low excess density—2–3 orders of magnitude smaller than rivers—turbidity currents can ascend topographic slopes several times their flow thickness (i.e., superelevation). However, existing predictive models used to estimate run-up height are either derived from 2D flume experiments and/or numerical simulations (B. Kneller & McCaffrey, 1999; Lane-Serff et al., 1995; Muck & Underwood, 1990; Rottman et al., 1985), assuming orthogonal flow-slope interactions. Therefore, different physiographic configurations, such as flow incidence angle onto the slope and slope gradient, are not accounted for in these estimates.

Here, we introduce a new analytical model, informed by and validated against 3D physical experiments, which predicts the maximum run-up height of turbidity currents across a spectrum of slope gradients and flow incidence angles. This model provides improved accuracy for natural configurations and can inform submarine geohazard assessments and develop more robust design criteria for the routing and placement of seafloor infrastructure.

2. Existing Models on the Estimation of Maximum Run-Up Height

Two-dimensional flume experiments demonstrate that the body of density currents encountering a frontal topography may run up 1.5–2.5 times flow thickness (Rottman et al., 1985). A simplified numerical model by Muck and Underwood (1990), assuming a full conversion of kinetic energy to potential energy and frictional

Project administration: Ru Wang, David M. Hodgson
Resources: Ru Wang, Ed Keavney, Helena C. Brown, Gareth M. Keevil
Software: Ru Wang
Supervision: Jeff Peakall, David M. Hodgson
Validation: Ru Wang, Mia Hughes
Visualization: Ru Wang, Mia Hughes
Writing – original draft: Ru Wang
Writing – review & editing: Ru Wang, Mia Hughes, Jeff Peakall, David M. Hodgson

dissipation, predicted a maximum run-up height of 1.53 times flow thickness, validated by saline density current experiments. B. Kneller and McCaffrey's (1999) model is the most widely used method to estimate maximum run-up height, which incorporates density stratification and vertical velocity variations. In this model, the maximum run-up elevation h_{max} of a fluid parcel of the current at initial height z is the sum of its initial elevation and its height gain, given by $h_{max} = z + \frac{\rho_z u_z^2 (1-E)}{2g\Delta\rho_z}$, where u_z is velocity normal to the slope at height z, g is gravitational acceleration, ρ_z and $\Delta\rho_z$ are flow density and density contrast with ambient fluid, respectively, and E represents proportion of frictional energy loss relative to the initial kinetic energy. The overall maximum run-up height, H_{max}, is the maximum of all h_{max} values.

3. Physical Experiments

Eighteen experiments were undertaken in a 10 m long, 2.5 m wide, and 0.6 m deep tank, to assess the run-up of low-density (0.3% excess bulk density), turbulent, subcritical, saline-driven gravity currents interacting with a planar ramp (1.5 m wide and 3 m from the inlet), as a function of ramp gradient (between 20 and 40°) and incidence angle (15–90°) (Text S1 and Figure S1 in Supporting Information S1; Keavney et al., 2025; Wang et al., 2025a). Such flow densities, and criticality, are typical of natural turbidity currents (e.g., Konsoer et al., 2013; Peakall & Sumner, 2015). The impinging three-dimensional flows were unable to surmount the ramp. Maximum run-up elevations were recorded using four high-resolution video cameras. The experiments reveal that maximum run-up height, H_{max} (cf. Edwards et al., 1994; Pantin & Leeder, 1987), increases strongly with greater incidence angles, but is a markedly non-linear function of slope gradient (Figures 1a and 1b). The most extreme height reached across all experiments was 3.3 times flow thickness. The height in the frontal experiments was ca. 2.5–2.7 times flow thickness, markedly more than the highest values predicted by B. Kneller and McCaffrey (1999) (Text S2 in Supporting Information S1) and Muck and Underwood (1990) methods (2.1 and 1.53 times flow thickness, respectively), and slightly higher than the upper limit of the prediction range (1.5–2.5) by Rottman et al. (1985) (Figure 1a). The observed relationships demonstrate that previous work greatly underpredicts maximum heights, and that orthogonal slopes are a very poor guide to run-up heights at other incidence angles. In addition, they demonstrate that slope gradient has a complicated relationship with maximum run-up height, where 30° slopes typically have higher run-up heights than either 20° or 40° slopes (Figure 1a). The experiments show that a predictive model of this phase space is required for the application of maximum run-up height modeling for risk assessment.

4. Analytical Modeling

4.1. Derivation of the Analytical Model in 3D Unconfined Setting

The experimental data (Figure 1a) challenges existing 2D methods for estimating upslope run-up heights. We propose a new analytical model that incorporates the effects of slope gradient (θ) and flow incidence angle (φ). The model develops the B. Kneller and McCaffrey (1999) approach based on energy balance principles, accounting for kinetic energy, potential energy, work done by pressure, as well as frictional and turbulent dissipation (Allen, 1985; see Text S3 in Supporting Information S1 for details on the predictive model derivation). Like the Kneller-McCaffrey method, this model considers a fluid parcel at initial height z upon reaching the slope, approximating the fluid parcel as retaining its density and structure throughout its journey up the ramp. This models the fluid parcel as a classical point particle (cf. B. Kneller & McCaffrey, 1999). These broad approximations circumvent the need to solve nonlinear hydrodynamic equations.

We assume an initial velocity $\vec{U} = (u_z, 0, 0)$ for each parcel of fluid meeting the ramp, with the x, y, and z axes aligned with the downstream, cross-stream and vertical directions, respectively (Figure S3a in Supporting Information S1). The flow velocity u_z is averaged over all horizontal locations, with the subscript denoting its remaining dependence on vertical position z. The predicted run-up height for a fluid parcel at initial height z is

$$h_{max}(z) = z + \frac{\frac{1}{2}\rho_z u_z^2 \sin^2\varphi\left(\cos^2\theta + S\sin^2\theta\right) + \Delta E_{gain}}{\Delta\rho_z g + \frac{F_{ave}}{\sin\alpha}} \quad (1)$$

The z subscripts refer to the density and velocity at height z. In the above equation, ΔE_{gain} models the energy gained from internal pressure and interactions of the fluid parcel with neighboring fluid parcels; S is a

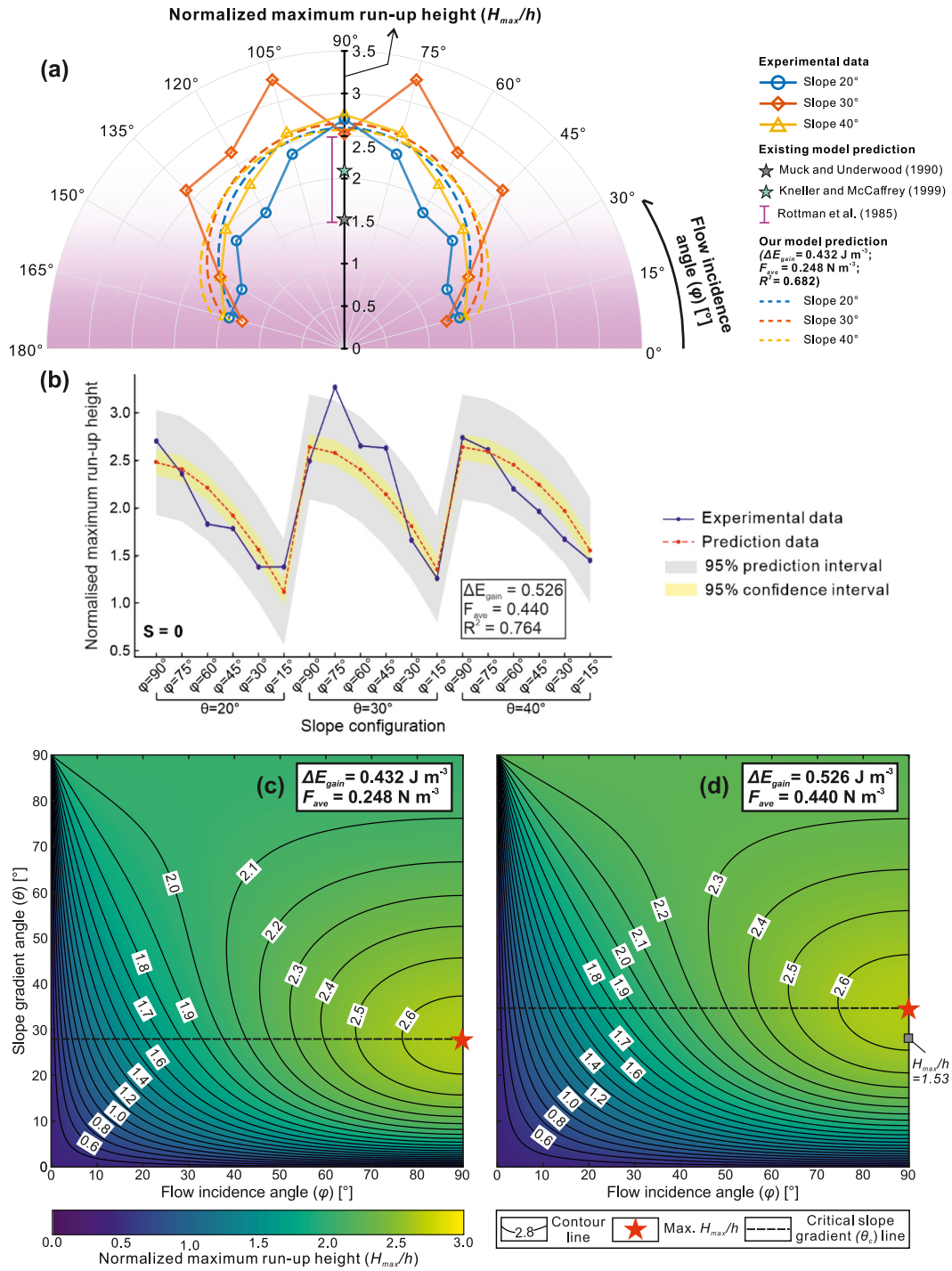

Figure 1. Polar diagram (a) and plots (b) illustrating the observed and predicted values of normalized maximum run-up height upslope in 18 ramp experiments. The best-fit values of ΔE_{gain} and F_{ave} with the observed experimental data points used in our analytical model prediction in (a) are derived on the condition that $\overline{H_{\text{max}}}$ (Slope 30°) > $\overline{H_{\text{max}}}$ (Slope 40°) > $\overline{H_{\text{max}}}$ (Slope 20°) (The overbar on H_{max} denotes the averaged value of the corresponding quantity) whereas the values in (b) are chosen when the condition is more relaxed. In (a), the radial axis represents magnitude of (normalized) run-up height and the angular axis is flow incidence angle relative to the slope. Run-up heights for obtuse incidence angles are displayed symmetrically to measured acute values. (c, d) Contour maps of modeled normalized maximum run-up height, H_{max}/h, across the full flow incidence angle onto the slope (φ), and slope gradient (θ) parameter space, with the input variables set to constants and optimized ΔE_{gain} and F_{ave}. Gray square in (d) represents the Muck and Underwood (1990) prediction.

dimensionless collision factor ranging from 0 to 1, characterizing the fraction of kinetic energy associated with the normal component of the initial velocity that contributes to H_{max}, likely a function of flow properties and topographic slope substrate; F_{ave} is average dissipative force per unit volume, due to frictional and turbulent dissipation, acting in the direction opposed to the fluid parcel's velocity. Its approximate magnitude can be estimated as $F_{ave} = \mu N$, where μ is the frictional coefficient and N is the normal contact force from the ramp, which should be equal to the component of the weight (per unit volume) normal to the ramp: $N = \rho g' \cos\theta$. Angle $\alpha = \tan^{-1}(\sin\varphi \tan\theta)$ represents the "effective slope" of the ramp in the downstream (x) direction in the vertical (x, z) plane (Figure S3d in Supporting Information S1).

The overall H_{max} is the maximum value of $h_{max}(z)$ over the interval $0 \le z \le h$, where h is the flow thickness of the current body. This maximum occurs when

$$\frac{d}{dz}\left(z + \frac{\frac{1}{2}\rho_z u_z^2 \sin^2\varphi\left(\cos^2\theta + S\sin^2\theta\right) + \Delta E_{gain}}{\Delta\rho_z g + \frac{F_{ave}}{\sin\alpha}}\right) = 0 \tag{2}$$

or, where no local maximum exists, the global maximum occurs infinitesimally close to the top of the flow. In the latter case, the second term in Equation 1 is negligible, and the maximum run-up height is almost equal to the flow thickness h.

To facilitate comparison to natural turbidity currents, we normalize $h_{max}(z)$ by the flow thickness h:

$$\frac{h_{max}(z)}{h} = \frac{z}{h} + \frac{\frac{1}{2}\rho_z u_z^2 \sin^2\varphi\left(\cos^2\theta + S\sin^2\theta\right) + \Delta E_{gain}}{\left(\Delta\rho_z g + \frac{F_{ave}}{\sin\alpha}\right)h} \tag{3}$$

If a local maximum exists then H_{max}/h is the value at this maximum, otherwise H_{max}/h is $h_{max}(h)/h \approx 1$, in which case the flow makes negligible up-ramp progress.

Note that the collision factor S, average dissipative force F_{ave}, and energy gain from the surrounding fluid ΔE_{gain} are at this stage unknown variables, each requiring their own estimation, and are likely themselves to depend on the initial velocity, density and the angles φ and θ. In the present study, they are approximated at zeroth order and treated as constants.

4.2. Comparison of Analytical-Model Predictions With Observed Experimental Data

The validity of the analytical model is tested by comparing run-up height predictions with the observed values for the 18 experiments, to approximate the dependence of (normalized) maximum run-up height on flow incidence angle and slope gradient. The purpose is to provide a first-order method of run-up estimation for all slope-incidence angle configurations. Given the approximations made in the model and the turbulent nature of the flow ($Re \approx 3000$), only a loose fit to the data is expected. A full Computational Fluid Dynamics simulation would be too computationally heavy and require similar input uncertainties.

In experiments, the dilute head of the density current is the main contributor to the maximum run-up height (Figure S2 in Supporting Information S1). Therefore, input values representative of those measured in the physical experiments in the first 5 s after the current head were substituted into the model ($z = 0.045$ m, $\rho_z = 999.8$ kg m^{-3}, $\Delta\rho_z = 0.22$ kg m^{-3}, $u_z = 0.0243$ m s^{-1}; note U_{max} position at $z = 0.04$ m; the flow height, h, was 0.11 m). The time-averaged downstream velocity profile from the UVP measurements, and density profile of the experimental density currents at 3 m downstream from the channel mouth along the channel-basin centerline were obtained by averaging measurements over 5 s, after the current head (Figure S2a in Supporting Information S1). We then split the vertical profiles into 27 regularly spaced fluid parcels (0.005 m), and substituted into the model. The values of density and velocity at $z = 0.045$ m is ultimately used herein, which represent the combination of z, $\Delta\rho_z$ and u_z values that typically leads to the maximum run-up height H_{max}. However, values for the energy gain ΔE_{gain}, averaged dissipative force F_{ave} and collision factor S were not measured in the physical experiments. For simplicity, S is assumed to be 0, meaning none of the kinetic energy associated with the component of the velocity normal to the ramp was converted into gravitational potential energy. The best-fit

values with the observed experimental data points for the remaining two parameters were $\Delta E_{gain} = 0.432$ J m^{-3} and $F_{ave} = 0.248$ N m^{-3} if parameters are chosen such that $\overline{H_{max}}$ (Slope 30°) > $\overline{H_{max}}$ (Slope 40°) > $\overline{H_{max}}$ (Slope 20°) (or $\Delta E_{gain} = 0.526$ J m^{-3} and $F_{ave} = 0.440$ N m^{-3} if the condition is more relaxed; Figures 1a and 1b, respectively). Note that the initial guess for F_{ave} is set to be $\mu\rho g'$ when looking for the best-fit values, whereby $\mu = 0.004$, typical in plexiglass experiments (Davarpanah Jazi et al., 2020). Figures 1c and 1d are contour maps of modeled normalized H_{max}/h, as a function of flow incidence angle onto the slope (φ) and slope angle (θ), using the input values above, respectively.

The analytical model (Figure 1) captures the first-order dependence of normalized H_{max}/h as a function of flow incidence angle and slope gradient. When the slope gradient is constant, the predicted H_{max}/h increases with a higher flow incidence angle, approximately reproducing the observed positive relationship between values H_{max}/h and the flow incidence angle in the physical experiments (Figures 1a and 1b). The model (Figures 1c and 1d) predicts a critical slope gradient ($\theta = 34.5°$ or 28.0°), at which H_{max}/h reaches its maximum of 2.66. This trend is approximately consistent with the experimental observations in an oblique setting of higher H_{max}/h for a slope of 30° compared to 20° and 40° (Figure 1a). However, the maximum H_{max}/h is lower than the observed maximum (ca. 3.3 times flow thickness in Experiment θ30° φ75°). This discrepancy in maximum H_{max}/h might be attributed to: (a) underprediction of S, reflecting a fraction of the kinetic energy associated with the component of the velocity normal to the ramp being converted into gravitational potential energy in the experiment; (b) lateral variability of the maximum run-up line in the experiments (Wang et al., 2025a) likely led to some fluid parcels having particularly large up-slope velocity components, and a higher H_{max} value than modeled predictions; (c) the frictional coefficient, $\mu = 0.004$, may have been overestimated, and therefore a lower normalized H_{max}/h predicted; and (d) in some cases, an H_{max} is not reached at $z = 0.045$ m, and therefore the maximum run-up height might be achieved at a different height within the flow. See further discussion in the Sensitivity Analysis (Section 4.3).

4.3. Evaluation of the Analytical Model by Field Data

To simulate the normalized maximum run-up height of a natural turbidity current, we assume a dilute flow ($\rho_s = 1{,}060$ kg m^{-3}; $\Delta\rho_s = 30$ kg m^{-3}) that has an initial downstream velocity of 5 m s^{-1} and flow height of 39 m ($u = 5$ m s^{-1}; $h = 39$ m). Here, for simplicity, constant values are used, due to the absence of coupled velocity and density profiles for unconfined turbidity currents recorded in the field (only velocity profiles exist; Lintern et al., 2016; Hill & Lintern, 2022). The energy gain from the internal pressure of the nearby fluid parcels is poorly known. $\Delta E_{gain} = 9{,}600$ J m^{-3} is chosen as it is tested to yield a realistic output of (normalized) maximum run-up height similar to the experimental results (Figure 1). Here F_{ave} varies from 0 to 3 N m^{-3}, approximately corresponding to the case whereby the friction coefficient $\mu = 0$, 0.001, 0.005, and 0.01, respectively. These input quantities are within observational ranges from field-scale turbidity currents (e.g., Azpiroz-Zabala et al., 2024; Lamb et al., 2008; Symons et al., 2017). In particular, the friction coefficient is demonstrated to vary from 10^{-3} to 10^{-2} (Davarpanah Jazi et al., 2020; Parker et al., 1987), although $\mu \approx 5 \times 10^{-3}$ is used for field-scale turbidity currents (e.g., Parker et al., 1986; Pirmez & Imran, 2003).

We conducted sensitivity analysis to explore the effect of different input variables incorporated in Equation 3 on the normalized H_{max}/h for a specific topographic configuration ($\theta = 45°$ and $\varphi = 90°$) with the above-mentioned input variables set as a base case and S equal to 0.5 (Figure 2a). Increasing the excess density difference or averaged dissipative force F_{ave} reduces H_{max}/h, whereas increasing the remaining input parameters such as S or ΔE_{gain} increases H_{max}/h. Initial downstream flow velocity U and excess density difference $\Delta\rho_s/\rho_s$ are the most influential factors affecting H_{max}/h, collision factor S and energy gain from internal pressure of nearby fluid parcels ΔE_{gain} are moderately sensitive while the averaged dissipative force F_{ave} has the least impact.

We explored the effect of flow incidence angle onto the slope (φ) and slope gradient (θ) on (normalized) maximum run-up height with covarying averaged dissipative force F_{ave} (Figures 2b–2e). Taking $F_{ave} = 1.5$ N m^{-3} (Figure 2d) indicates that an increase in flow incidence angle with the same slope gradient leads to a higher H_{max}/h. This is because higher flow incidence angles correspond to better alignment between the average flow velocity and the updip direction. However, the impact of the angle of the topographic slope is more complicated when the flow incidence angle is kept uniform. For zero average dissipative force F_{ave} (Figure 2b), when the friction or turbulent dissipation is negligible, a steeper slope gradient leads to lower H_{max}/h. For non-zero average

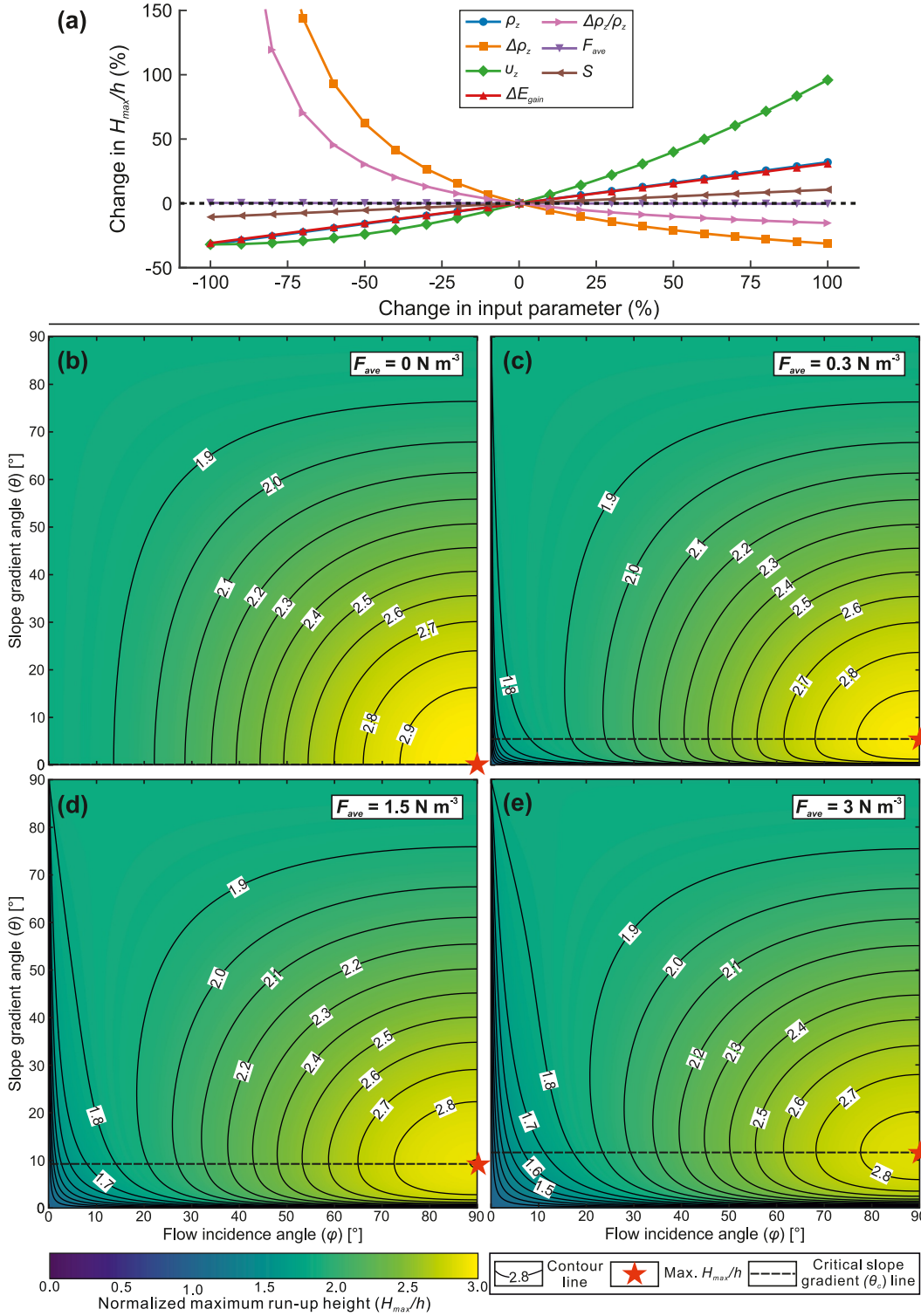

Figure 2. (a) Sensitivity analysis of the impact of initial downstream flow velocity U, excess density difference $\Delta\rho_s/\rho_s$, collision factor S, energy gain from internal pressure of nearby fluid parcels ΔE_{gain} and the averaged dissipative force F_{ave} on the normalized maximum run-up height. (b–e) Analytical model results for normalized H_{max}/h of turbidity currents interacting with a topographic slope with averaged dissipative force F_{ave} varying from 0 to 3 N m^{-3} approximately corresponding to cases where the frictional coefficient $\mu = 0$, 0.001, 0.005 and 0.01, respectively. In each panel map, contours of normalized maximum run-up height, H_{max}/h, as a function of the flow incidence angle onto the slope (φ), and slope angle (θ), with other variables set to constants typical of field-scale turbidity currents. For all panel maps, $S = 0$ assuming a maximal collision model and $\Delta E_{\text{gain}} = 9{,}600$ J m^{-3}.

dissipative force F_{ave} (Figures 2c–2e), a critical slope gradient θ exists, whereby the normalized H_{max}/h achieves its maximum, that is, increasing the slope gradient for a given flow incidence angle results in an increase then decrease in the normalized H_{max}/h. Crucially, the critical slope gradient θ_c increases with rising F_{ave}.

5. Discussion

5.1. Comparison With Existing 2D Predictive Models

The greater maximum run-up heights of density currents observed in our laboratory experiments compared to 2D predictive models (Figure 1a) challenge the validity of existing approaches in natural settings. Potential reasons for the discrepancy include: (a) the fluid parcel that reaches H_{max} is pushed forward by the flow behind it (and the pressure gradient due to the density gradient between the saline and ambient water); and (b) in an unconfined turbidity current setting, the downstream velocity and the vertical and cross-stream velocity components contribute to the initial kinetic energy, which leads to a greater final potential energy and consequently comparatively higher upslope run-up heights. Critically, a fluid parcel that reaches H_{max} must receive additional energy from the force of the flow behind it, and from the pressure gradient at the boundary between the saline and ambient water, allowing it to reach a greater elevation than the B. Kneller and McCaffrey (1999) approach predicts. Our analytical model addresses this issue by adding a contribution to the energy density, ΔE_{gain}, modeling the zeroth order effect of pressure gradients in the fluid.

In contrast to previous 2D models that only addressed the orthogonal flow-slope interaction, our new analytical model, validated against large-scale 3D physical experiments, highlights the importance of both topographic slope angle and flow-slope incidence angle on the run-up height. The effect of these two parameters is considered via modeling their contribution to both the available and dissipated energy of a fluid parcel reaching H_{max}, which is mainly achieved by incorporating the trigonometric decomposition of initial velocity (Figures S3b–S3d in Supporting Information S1) and modeling the energy losses to friction and/or turbulent dissipation.

5.2. Influence of Slope Gradient and Flow Incidence Angle on the Magnitude of Maximum Run-Up Height

Our model predicts a highly non-linear dependence of run-up height on slope angle, due to its direction-dependent modeling of the available kinetic energy, in addition to assuming energy dissipation increases with the distance traveled by each fluid parcel. Without these two considerations, the predicted maximum run-up height would be independent of slope angle (Allen, 1985; Pantin & Leeder, 1987). In contrast to previous models, our predictions, informed by and validated against our laboratory experimental results (Figures 1 and 2b–2e), reveal a critical slope gradient θ_c for non-zero average dissipative force F_{ave}, with θ_c increasing with rising F_{ave}. This complicated θ dependence is ascribed to competing effects of: (a) increasing θ decreases alignment between the average flow direction and the up-dip direction, lowering the run-up height (Figures S3b and S3c in Supporting Information S1); and (b) increasing θ reduces the distance to travel on the slope surface to achieve the same vertical run-up height, meaning less energy is lost to friction or turbulent dissipation, increasing the run-up height. In the regime $\theta < \theta_c$ with the same flow incidence angle relative to the slope, the influence of the average dissipative force dominates and thus a steeper slope gradient is associated with higher H_{max}/h. In the regime $\theta > \theta_c$ with the same flow incidence angle relative to the slope, the influence of the collision factor dominates and thus a steeper slope gradient is associated with lower H_{max}/h.

The flow incidence angle has a marked impact on maximum run-up height. Our analytical model and laboratory experiments (Figures 1a and 2b–2e) show more oblique flow interactions with the topographic slope (e.g., 15°–45° incidence angles) tend to have lower maximum run-up heights because of less topographic containment and therefore reduced up-dip velocity component (e.g., Snyder et al., 1985; Straub et al., 2011). In contrast, near-perpendicular interactions (e.g., 75°–90°) allow more initial kinetic energy to be converted into gravitational potential energy. Our experimental results (Figures 1a and 1b; Figure S4 and Text S4 in Supporting Information S1) also indicate that a critical flow incidence angle φ_c exists at less than 90° at which there is a pronounced boost in superelevation, leading to the highest run-up height. This is likely a consequence of variations in the cross-stream velocity component, which effectively changes the local incidence angle of the fluid parcel relative to the ramp. A change in the incidence angle by some amount $\Delta\varphi$ results in a maximum when $\varphi = 90° - \Delta\varphi$, as opposed to when $\varphi = 90°$.

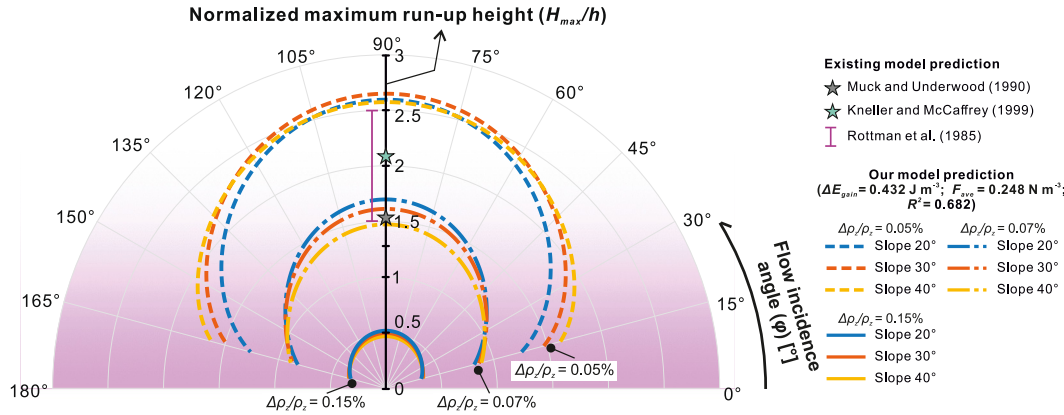

Figure 3. Polar plot illustrating how density stratification affects local run-up heights, showing the predicted normalized maximum run-up heights for three excess density values, at flow heights, $z = 0.01$, 0.04, and 0.045 m. Based on the analytical model prediction from the laboratory experiments. See Text S5 in Supporting Information S1 for further details.

5.3. Influence of Density Stratification on Run-Up

The effects of density stratification on run-up, at different heights within the experimental flow, are shown in Figure 3. The densest, basal components have low run-up heights, whilst run-up heights are greatest just above the velocity maximum (Figure 3). Sediment-laden flows typically exhibit enhanced stratification relative to saline flow experiments (Dorrell et al., 2014; Wells & Dorrell, 2021), thus will likely produce greater variation in run-up, with height in the flow. Experimental turbidity currents show that the velocity maximum can coincide with greater densities than in saline flows (Wells & Dorrell, 2021, their Figure 3), suggesting they should exhibit higher maximum run-up. However, turbidity currents also undergo sedimentation as they interact with slopes. As noted earlier, there is a lack of coupled velocity-density profiles for natural unconfined turbidity currents. Once such profiles become available, the model will enable run-up heights to be directly compared to saline flows, assuming conservative flow.

5.4. Implications for Reconstructing Submarine Landscapes

Reconstructing the configuration of ancient submarine landscapes requires excellent understanding of the deposits of flow-topography interactions. Our new analytical model for calculating flow run-up heights on different slope orientations can be applied to outcrop and subsurface data sets to better constrain basin physiography (gradient and aspect) at the time of deposition. We show that relatively minor changes in slope gradient and incidence angle have a substantial influence on run-up height, and therefore depositional patterns, which might help to explain the complicated onlap geometries documented in many confined basin-fills (e.g., Bakke et al., 2013). We recommend attempting to apply our model in ancient outcrop settings where bed-scale sedimentology, paleoflow directions, and stratal geometry can be documented with three-dimensional control (e.g., Soutter et al., 2019).

5.5. Implications for Seafloor Geohazards

Destructive particulate turbidity currents pose a serious hazard to high-value seafloor infrastructure, particularly in submarine slope settings where mitigation, rerouting or repairs are costly (e.g., Bricheno et al., 2024). The systematic underestimation of run-up heights by 2D models (Figure 1a) suggests that existing geohazard assessments substantially underpredict the spatial extent of turbidity current impact (Figure 3). Our new analytical model, incorporating gradient, incidence angle, and flow density stratification, provides a more accurate basis for evaluating the interaction of turbidity currents with seafloor topography (Figure 3). Identifying a critical slope gradient that maximizes run-up height (Figures 2c–2e) enhances predictions of increased hazard potential. The strong sensitivity of run-up to flow incidence angles (Figures 1 and 2b–2e) highlights the importance of 3D bathymetric mapping and flow path modeling in routing infrastructure away from areas of increased risk from turbidity currents. The framework to estimate run-up height on 3D topographic slopes in this work provides an

improved tool for forecasting the spatial extent of turbidity current impacts. Future integration of our model prediction with 3D reliability analysis (e.g., Wu et al., 2025) can aid the quantitative assessment of the infrastructure failure probabilities under complex flow-topography interactions. Further coupling with machine learning-based early warning systems (e.g., Zhang et al., 2022) may enable real-time geohazard mitigation for submarine cables and pipelines.

6. Conclusions

Existing predictive models based on 2D confined turbidity currents interacting with topography are shown to substantially underestimate run-up heights. Consequently, existing predictive model estimates are not fit for purpose when forecasting run-up heights during risk assessments at a time when critical seafloor infrastructure is rapidly expanding. A new analytical model that incorporates trigonometric decomposition of initial velocity, energy gain from the pressure gradients in the fluid, and modeling of energy loss to friction and/or turbulent dissipation, captures the key dynamics of low-density turbidity current interactions with topography in 3D settings. This analytical model, validated against 3D physical experiments, provides a more accurate predictive framework for run-up heights across all slope gradient and flow incidence angle configurations. A critical slope gradient exists whereby the maximum run-up height reaches its highest value compared to both gentler and steeper slopes. Run-up can also be examined as a function of the density stratification within a flow. Results can be applied to inform the routing and installation of seafloor infrastructure to mitigate seafloor geohazards, and for more accurate interpretation of submarine landscapes and their deposits.

Conflict of Interest

The authors declare no conflicts of interest relevant to this study.

Data Availability Statement

The maximum run-up height data for the ramp experiments used in this study are obtained from the high-resolution videos, which are publicly available and can be downloaded from Wang et al. (2025b). The analysis codes developed in this study are available in Wang et al. (2026).

Acknowledgments
We thank the LOBE 3 Joint Industry Programme partners (AkerBP, BP, Equinor, Hess, Petrobras, Petrochina, TotalEnergies, Vår Energi, Woodside), and Dave Mohrig, Editor Neil Ganju, and an anonymous reviewer for their helpful comments.

References

Allen, J. R. L. (1985). *Principles of physical sedimentology* (pp. 223–242). George Allen & Unwin.

Azpiroz-Zabala, M., Sumner, E. J., Cartigny, M. J. B., Peakall, J., Clare, M. A., Darby, S. E., et al. (2024). Benthic biology influences sedimentation in submarine channel bends: Coupling of biology, sedimentation and flow. *The Depositional Record*, *10*, 159–175. https://doi.org/10.1002/dep2.265

Bakke, K., Kane, I. A., Martinsen, O. J., Petersen, S. A., Johansen, T. A., Hustoft, S., et al. (2013). Seismic modeling in the analysis of deep-water sandstone termination styles. *AAPG Bulletin*, *97*(9), 1395–1419. https://doi.org/10.1306/03041312069

Bricheno, L., Yeo, I., Clare, M., Hunt, J., Griffiths, A., Carter, L., et al. (2024). The diversity, frequency and severity of natural hazard impacts on subsea telecommunication networks. *Earth-Science Reviews*, *259*, 104972. https://doi.org/10.1016/j.earscirev.2024.104972

Davarpanah Jazi, S., Wells, M. G., Peakall, J., Dorrell, R. M., Thomas, R. E., Keevil, G. M., et al. (2020). Influence of Coriolis force upon bottom boundary layers in a large-scale gravity current experiment: Implications for evolution of sinuous deep-water channel systems. *Journal of Geophysical Research: Oceans*, *125*(3), e2019JC015284. https://doi.org/10.1029/2019JC015284

Dorrell, R. M., Darby, S. E., Peakall, J., Sumner, E. S., Parsons, D. R., & Wynn, R. B. (2014). The critical role of stratification in submarine channels: Implications for channelization and long run-out flows. *Journal of Geophysical Research: Oceans*, *119*(4), 2620–2641. https://doi.org/10.1002/2014JC009807

Edwards, D. A., Leeder, M. R., Best, J. L., & Pantin, H. M. (1994). On experimental reflected density currents and the interpretation of certain turbidites. *Sedimentology*, *41*(3), 437–461. https://doi.org/10.1111/j.1365-3091.1994.tb02005.x

Hill, P. R., & Lintern, D. G. (2022). Turbidity currents on the open slope of the Fraser Delta. *Marine Geology*, *445*, 106738. https://doi.org/10.1016/j.margeo.2022.106738

Keavney, E., Peakall, J., Wang, R., Hodgson, D. M., Kane, I. A., Keevil, G. M., et al. (2025). Unconfined gravity current interactions with orthogonal topography: Implications for combined-flow processes and the depositional record. *Sedimentology*, *72*(1), 67–99. https://doi.org/10.1111/sed.13227

Kneller, B., & Buckee, C. (2000). The structure and fluid mechanics of turbidity currents: A review of some recent studies and their geological implications. *Sedimentology*, *47*(s1), 62–94. https://doi.org/10.1046/j.1365-3091.2000.047s1062.x

Kneller, B., Edwards, D., McCaffrey, W., & Moore, R. (1991). Oblique reflection of turbidity currents. *Geology*, *14*(3), 250–252. https://doi.org/10.1130/0091-7613(1991)019<0250:OROTC>2.3.CO;2

Kneller, B., & McCaffrey, W. (1999). Depositional effects of flow nonuniformity and stratification within turbidity currents approaching a bounding slope: Deflection, reflection, and facies variation. *Journal of Sedimentary Research*, *69*(5), 980–991. https://doi.org/10.2110/jsr.69.980

Kneller, B. C., Bennett, S. J., & McCaffrey, W. D. (1997). Velocity and turbulence structure of density currents and internal solitary waves: Potential sediment transport and the formation of wave ripples in deep water. *Sedimentary Geology*, *112*(3–4), 235–250. https://doi.org/10.1016/S0037-0738(97)00031-6

Konsoer, K., Zinger, J., & Parker, G. (2013). Bankfull hydraulic geometry of submarine channels created by turbidity currents: Relations between bankfull channel characteristics and formative flow discharge. *Journal of Geophysical Research: Earth Surface*, *118*(1), 216–228. https://doi.org/10.1029/2012JF002422

Lamb, M. P., Parsons, J. D., Mullenbach, B. L., Finlayson, D. P., Orange, D. L., & Nittrouer, C. A. (2008). Evidence for superelevation, channel incision, and formation of cyclic steps by turbidity currents in Eel Canyon, California. *Geological Society of America Bulletin*, *120*(3–4), 463–475. https://doi.org/10.1130/B26184.1

Lane-Serff, G. F., Beal, L. M., & Hadfield, T. D. (1995). Gravity current flow over obstacles. *Journal of Fluid Mechanics*, *292*, 39–54. https://doi.org/10.1017/S002211209500142X

Lintern, D. G., Hill, P. R., & Stacey, C. (2016). Powerful unconfined turbidity current captured by cabled observatory on the Fraser River delta slope, British Columbia, Canada. *Sedimentology*, *63*(5), 1041–1064. https://doi.org/10.1111/sed.12262

Muck, M. Y., & Underwood, M. B. (1990). Upslope flow of turbidity currents: A comparison among field observations, theory, and laboratory methods. *Geology*, *18*(1), 54–57. https://doi.org/10.1130/0091-7613(1990)018<0054:UFOTCA>2.3.CO;2

Pantin, H. M., & Leeder, M. R. (1987). Reverse flow in turbidity currents: The role of internal solitons. *Sedimentology*, *34*(6), 1143–1155. https://doi.org/10.1111/j.1365-3091.1987.tb00597.x

Parker, G., Fukushima, Y., & Pantin, H. M. (1986). Self-accelerating turbidity currents. *Journal of Fluid Mechanics*, *171*, 145–181. https://doi.org/10.1017/S0022112086001404

Parker, G., Garcia, M., Fukushima, Y., & Yu, W. (1987). Experiments on turbidity currents over an erodible bed. *Journal of Hydraulic Research*, *25*(1), 123–147. https://doi.org/10.1080/00221688709499292

Peakall, J., & Sumner, E. J. (2015). Submarine channel flow processes and deposits: A process-product perspective. *Geomorphology*, *244*, 95–120. https://doi.org/10.1016/j.geomorph.2015.03.005

Pirmez, C., & Imran, J. (2003). Reconstruction of turbidity currents in Amazon Channel. *Marine and Petroleum Geology*, *20*(6–8), 823–849. https://doi.org/10.1016/j.marpetgeo.2003.03.005

Rottman, J. W., Simpson, J. E., Hunt, J. C. R., & Britter, R. (1985). Unsteady gravity current flows over obstacles: Some observations and analysis related to the Phase II trials. *The Journal of Hazardous Materials*, *11*, 325–340. https://doi.org/10.1016/0304-3894(85)85044-5

Snyder, W. H., Thompson, R. S., Eskridge, R. E., Lawson, R. E., Castro, I. P., Lee, J. T., et al. (1985). The structure of strongly stratified flow over hills: Dividing-streamline concept. *Journal of Fluid Mechanics*, *152*, 249–288. https://doi.org/10.1017/S0022112085000684

Soutter, E. L., Kane, I. A., Fuhrmann, A., Cumberpatch, Z. A., & Huuse, M. (2019). The stratigraphic evolution of onlap in siliciclastic deep-water systems: Autogenic modulation of allogenic signals. *Journal of Sedimentary Research*, *89*(10), 890–917. https://doi.org/10.2110/jsr.2019.49

Straub, K. M., Mohrig, D., Buttles, J., McElroy, B., & Pirmez, C. (2011). Quantifying the influence of channel sinuosity on the depositional mechanics of channelized turbidity currents: A laboratory study. *Marine and Petroleum Geology*, *28*(3), 744–760. https://doi.org/10.1016/j.marpetgeo.2010.05.014

Symons, W. O., Sumner, E. J., Paull, C. K., Cartigny, M. J., Xu, J. P., Maier, K. L., et al. (2017). A new model for turbidity current behavior based on integration of flow monitoring and precision coring in a submarine canyon. *Geology*, *45*(4), 367–370. https://doi.org/10.1130/G38764.1

Wang, R., Hughes, M., Peakall, J., Hodgson, D. M., Keavney, E., Brown, H. C., & Keevil, G. M. (2026). New analytical model for forecasting turbidity current run-up heights: Implications for risk assessment of seafloor infrastructure on submarine slopes [Dataset]. *Zenodo*. https://doi.org/10.5281/zenodo.16883713

Wang, R., Peakall, J., Hodgson, D. M., Keavney, E., Brown, H. C., & Keevil, G. M. (2025a). Three-dimensional gravity current interactions with oblique slopes: Deflection, reflection and combined-flow behaviours. *Sedimentology*, *72*(7), 2121–2159. https://doi.org/10.1111/sed.70032

Wang, R., Peakall, J., Hodgson, D. M., Keavney, E., Brown, H. C., & Keevil, G. M. (2025b). Three-dimensional gravity current interactions with oblique slopes: Deflection, reflection and combined-flow behaviours [Dataset]. *Zenodo*. https://doi.org/10.5281/zenodo.13988491

Wells, M. G., & Dorrell, R. M. (2021). Turbulence processes within turbidity currents. *Annual Review of Fluid Mechanics*, *53*(1), 59–83. https://doi.org/10.1146/annurev-fluid-010719-060309

Wu, C., Wang, Z. Z., Goh, S. H., & Zhang, W. (2025). A methodology for three-dimensional slope reliability assessment considering spatial variability. *Journal of Geotechnical and Geoenvironmental Engineering*, *151*(5), 04025020. https://doi.org/10.1061/JGGEFK.GTENG-12986

Zhang, W., Li, H., Tang, L., Gu, X., Wang, L., & Wang, L. (2022). Displacement prediction of Jiuxianping landslide using gated recurrent unit (GRU) networks. *Acta Geotechnica*, *17*(4), 1367–1382. https://doi.org/10.1007/s11440-022-01495-8

References From the Supporting Information

Hodgson, D. M., Peakall, J., & Maier, K. L. (2022). Submarine channel mouth settings: Processes, geomorphology, and deposits. *Frontiers in Earth Science*, *10*, 790320. https://doi.org/10.3389/feart.2022.790320

Komar, P. D. (1971). Hydraulic jumps in turbidity currents. *Geological Society of America Bulletin*, *82*(6), 1477–1488. https://doi.org/10.1130/0016-7606(1971)82[1477:HJITC]2.0.CO;2

Marshall, C. R., Dorrell, R. M., Keevil, G. M., Peakall, J., & Tobias, S. M. (2023). On the role of transverse motion in pseudo-steady gravity currents. *Experiments in Fluids*, *64*(3), 63. https://doi.org/10.1007/s00348-023-03599-7

Nomura, S., Hitomi, J., De Cesare, G., Takeda, Y., Yamamoto, Y., & Sakaguchi, H. (2019). Sediment mass movement of a particle-laden turbidity current based on ultrasound velocity profiling and the distribution of sediment concentration. *Geological Society - Special Publications*, *477*(1), 427–437. https://doi.org/10.1144/SP477.19